NANO LETTERS

2009
Vol. 9, No. 2
601-606

Fabrication of Highly-Ordered TiO_2 Nanotube Arrays and Their Use in Dye-Sensitized Solar Cells

Tae-Sik Kang,[†,‡] Adam P. Smith,[†,‡] Barney E. Taylor,[†,‡] and Michael F. Durstock*[,†]

Air Force Research Laboratory, Materials & Manufacturing Directorate, Wright-Patterson Air Force Base, Ohio, and Universal Technology Corporation, Beavercreek, Ohio

Received September 16, 2008; Revised Manuscript Received November 26, 2008

ABSTRACT

Highly ordered TiO_2 nanotubes were successfully fabricated using a nanoporous alumina templating method. A modified sol−gel route was used to infiltrate the alumina pores with $Ti(OC_3H_7)_4$ which was subsequently converted into TiO_2 nanotubes. The average external diameter, tube lengths, and wall thickness achieved were 295 nm, 6−15 μm, and 21−42 nm, respectively. Diffraction data reveals that the nanotubes consist solely of the anatase phase. Dye-sensitized solar cells using TiO_2 nanotube arrays as the working electrode yielded power conversion efficiencies as high as 3.5% with a maximum incident photon-to-current conversion efficiency of 20% at 520 nm.

The development of solar energy devices as an alternative to nonrenewable power sources remains a focus of many groups seeking to provide solutions to rapidly increasing global energy demands. Photovoltaic systems based on organic materials and nanoparticle hybrid technologies are currently attracting widespread attention because of their potential for low cost and high-throughput manufacturing. Dye-sensitized solar cells (DSSCs) based on a TiO_2 working electrode with an adsorbed ruthenium complex have exhibited power conversion efficiencies over 11%[1] and remain one of the most promising device paradigms. Standard DSSCs rely on the fabrication of a mesoporous titania film with a very high internal surface area onto which a light-sensitizing dye is adsorbed. Upon illumination, the photoexcited dye injects an electron into the conduction band of the TiO_2. The electrons migrate through the TiO_2 network to be collected at the transparent electrode substrate. The light-sensitizing dye is subsequently regenerated electrochemically through an electrolyte, which is commonly based on an iodide/triiodide redox couple.

The mesoporous TiO_2 working electrode is typically based on a colloidal dispersion of TiO_2 nanoparticles that is deposited onto a surface and subsequently heat-treated. While the porosity of the resulting electrically continuous TiO_2 scaffold allows for high-surface area adsorption of the sensitizing dye, the random nature of this polycrystalline network can limit device performance. The ability to control the nanoscale architecture of the TiO_2 network is expected to positively impact solar cell performance by providing more direct migration pathways with improved charge transport efficiencies, as well as simplified device architectures. Furthermore, the creation of nanostructured electrodes is receiving widespread attention and could have significant influence in such diverse areas as photocatalysis, chemical sensing, and biotechnology.[2−5]

A number of fabrication methods have been used to form a variety of nanostructured TiO_2 features such as nanotubes, wires, dots, and pillars. Some of the fabrication techniques studied include anodic oxidation,[6] electrochemical lithography,[7] photoelectrochemical etching,[8] sol−gel processing,[9] hydrothermal synthesis,[10] and template synthesis.[11,12] Specifically, the formation of nanotubes and rods are attracting considerable attention due to their potentially superior photoelectrochemical and charge transport characteristics. It is envisioned that by replacing the traditional, mesoporous, randomly oriented TiO_2 network with ordered nanostructures comprised of nanotubes or rods oriented perpendicular to the substrate, increased charge transport would ensue resulting in improved device performance. Indeed, several groups have shown promise that ordered TiO_2 structures may ultimately lead to enhanced power conversion efficiencies. Fabrication of TiO_2 nanotube arrays via the direct anodization of titanium foil was first reported in 2001 by Grimes and co-workers.[13] By employing an array of oriented 6 μm-long TiO_2 nanotubes on titanium, devices achieving power conversion efficiencies as high as 5.44% under solar simulated conditions have been demonstrated.[14] Other related studies[15−23] have clearly shown that the performance char-

* To whom correspondence should be addressed. E-mail: Michael.Durstock@wpafb.af.mil.
† Wright-Patterson Air Force Base.
‡ Universal Technology Corporation.

10.1021/nl802818d CCC: $40.75
Published on Web 01/23/2009

acteristics of devices made from such titania nanotube structures are highly dependent upon a myriad of factors including nanotube morphology, geometry, surface modification, or other film preparation conditions. While many of these studies have focused on the direct anodization of titanium metal, other preparation techniques such as solution phase growth of nanorods have also shown much promise. In particular, Yang and co-workers have replaced the mesoporous TiO_2 film with an array of ZnO nanowires and have achieved a power conversion efficiency of 1.5%.[24] Additionally, Grimes and co-workers have very recently demonstrated a 5% efficient device using a solution phase growth technique of TiO_2 nanorods.[25]

Another strategy used in the fabrication of nanotubes or rods involves template-directed synthetic methods. Typically this involves the fabrication of a nanoporous template, backfilling with the material of interest, and then selectively removing the template to yield the resulting nanostructure. While many templates have been and continue to be investigated, the use of anodized alumina could provide a low-cost approach that is quite versatile in achieving controllable pore size and shape. Electrochemically anodizing aluminum in an aqueous, acidic solution results in the growth of an alumina film on the surface of the aluminum substrate. Under appropriate conditions, the alumina forms a highly ordered scaffold consisting of a nanostructured array of cylindrical pores oriented perpendicular to the aluminum substrate. The pore diameter and aspect ratio of this template can be controlled simply by adjusting the anodization conditions. A variety of approaches have been studied as a means to backfill the template including electrophoresis, electrochemical deposition, and solution infiltration, and this has resulted in a variety of oxide nanostructures being formed.[26−28] Electrodeposition typically results in the formation of nanorods. Chu and co-workers have had some success in fabricating TiO_2 nanotubes on a glass substrate by anodizing a sputtered aluminum substrate and using sol−gel infiltration.[29] Additionally, Yanagida and co-workers have used randomly oriented TiO_2 nanotubes to give devices with efficiencies greater than 6.5−7%.[30]

Despite the variety of approaches being examined for the creation of ordered structures, detailed studies relating the influence of electrode geometry on device performance are still needed. Toward that end, in this work we demonstrate a versatile technique of fabricating highly ordered TiO_2 nanotube arrays that provides the means of achieving simple geometry variations and that is based on nanoporous alumina template-directed growth and sol−gel infiltration. As will be discussed, achieving complete solution infiltration into the nanoporous template, and subsequently obtaining highly uniform TiO_2 nanotube arrays, is highly dependent upon the surface and solution preparation conditions. Preliminary device results obtained by transferring the nanotube arrays onto a transparent electrode substrate will also be discussed.

Nanoporous alumina templates were fabricated directly onto a high purity (99.999%) aluminum substrate through a series of electrochemical processing steps, as described below. The aluminum substrate was first washed by ultrasonic cleaning in ethanol and was then electropolished in an ethanol/water solution of perchloric acid (67/13/20 wt %, 2 min at 20 V and 7 °C) in order to remove surface defects. It was then galvanostatically anodized in an aqueous phosphoric acid solution (14 wt %, 5 h at 6 mA/cm^2 and 4 °C) followed by etching in an aqueous solution of phosphoric acid (5.3 wt%) and chromic acid (1.7 wt%) to remove the alumina film. The substrate was then anodized a second time under the same conditions and for an appropriate time interval (proportional to the channel length) to form the template. This two-step anodization process is utilized in order to obtain highly ordered alumina templates with cylindrical pores oriented perpendicular to the aluminum substrate. In order to promote pore-widening, the as-formed template was immersed in a 3 M NaOH solution for 3 min. This substrate is subsequently used as a template for the growth of titania nanotubes by vacuum infiltrating with a sol−gel precursor solution of titanium isopropoxide, $Ti(OC_3H_7)_4$, in ethanol (weight ratio of 3:1). After drying at room temperature for 12 h in an ambient environment (room temperature and approximately 54% relative humidity), the sample was heated in air for 30 min at 500 °C in order to complete the conversion to crystalline titania. Isolated TiO_2 nanotube arrays were finally obtained after removing the alumina template by etching in a 3 M NaOH solution for 13 min.

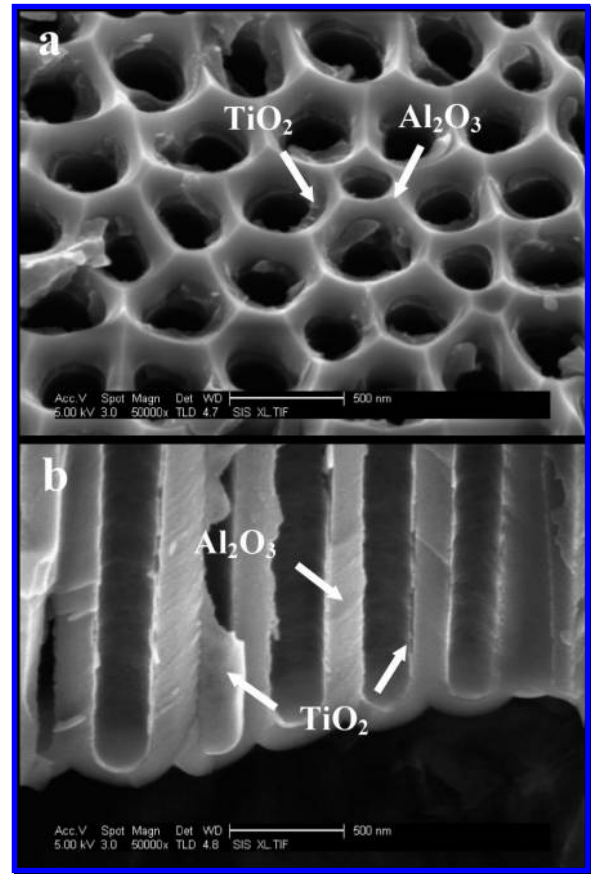

Figure 1. Field emission−SEM images of (a) top-down and (b) cross-sectional views of an alumina template after infiltration and annealing at 500 °C for 30 min. The average nanopore diameter and TiO_2 wall thickness are 295 and 21 nm, respectively.

Figure 1 shows representative field-emission SEM images (top-down and cross-sectional views) of this infiltrated

template after it has been heat-treated. As illustrated, the template consists of well-aligned, uniform, cylindrical pores (average of 295 nm in diameter) that extend down to the aluminum substrate. Between the bottom of the pores and the substrate, a thin barrier layer of alumina exists that is approximately 90 nm thick. The TiO_2 forms a conformal coating on the interior sidewalls of the pores, which is approximately 21 nm thick and that appears uniform, continuous, and dense. The top portion of this interior lining can be seen in Figure 1a, while the bottom is shown in Figure 1b. It is interesting to note that the uniformity of this conformal coating is a reflection of the favorable surface interactions between the as-prepared alumina template and the sol−gel solution. This is illustrated by a more careful consideration of the infiltration, drying, and conversion process. The solution used for infiltration of the pores is a mixture of $Ti(OC_3H_7)_4$ and ethanol in a 3:1 weight ratio. By taking into consideration their densities (0.937 g/cm^3 for $Ti(OC_3H_7)_4$ and 0.789 g/cm^3 for ethanol), it is calculated that a 28% volume change (shrinkage) would be observed upon drying and removal of the ethanol. Subsequent heat treatment at 500 °C for 30 min results in the formation of crystalline titania (as demonstrated below). By taking into consideration both the density (ρ) and molecular weight (MW) of $Ti(OC_3H_7)_4$ ($\rho = 0.937$ g/cm^3 and MW = 283.9 g/mol) and TiO_2 ($\rho = 3.84$ g/cm^3 and MW = 79.9 g/mol), it is calculated that a 93% shrinkage would be observed for this conversion process. The combined effects of both the removal of the ethanol and the high temperature conversion leads to an overall volume reduction of about 95%. For the nanotube and pore geometry shown in Figure 1 (pore diameter = 295 nm and nanotube wall thickness = 21 nm), the TiO_2 nanotube occupies approximately 26% of the pore volume. If it is assumed that a 95% volume reduction has occurred upon drying and conversion, as shown above, then an initial solution volume that is equal to 5 times the pore volume would have been required to produce the nanotubes with the observed wall thickness. This apparent conflict is understood by realizing the differences between the procedure used here and that used for traditional sol−gel processing. A typical sol solution of $Ti(OC_3H_7)_4$ includes both ethanol and water, plus a variety of other additives. The water acts to hydrolyze the $Ti(OC_3H_7)_4$ which then leads to the formation of TiO_2 particulates in solution (the sol) through a series of condensation reactions which, when brought to completion, results in the formation of the gel. The effects of varying these solution parameters on the structure of both the sol and the gel have been thoroughly investigated.[31] For the case here, the solution does not contain water and so hydrolysis does not occur to any significant extent in solution. However, drying of the infiltrated membrane is performed in an ambient environment (room temperature and approximately 54% relative humidity). During the drying process, the $Ti(OC_3H_7)_4$ is exposed to moisture thereby inducing hydrolysis and condensation and the associated volume contraction. Fresh solution continuously infiltrates the pores for further deposition ending in a uniform, conformal coating within the pore walls that gets converted to crystalline titania upon heat treatment. This is further emphasized by the fact that if a sol solution containing water is used instead, extremely poor infiltration and nonuniform deposition is observed. It should also be noted that the thin alumina barrier layer at the bottom of the pores prevents the TiO_2 from making direct contact to the aluminum substrate, a fact that will be discussed in more detail later.

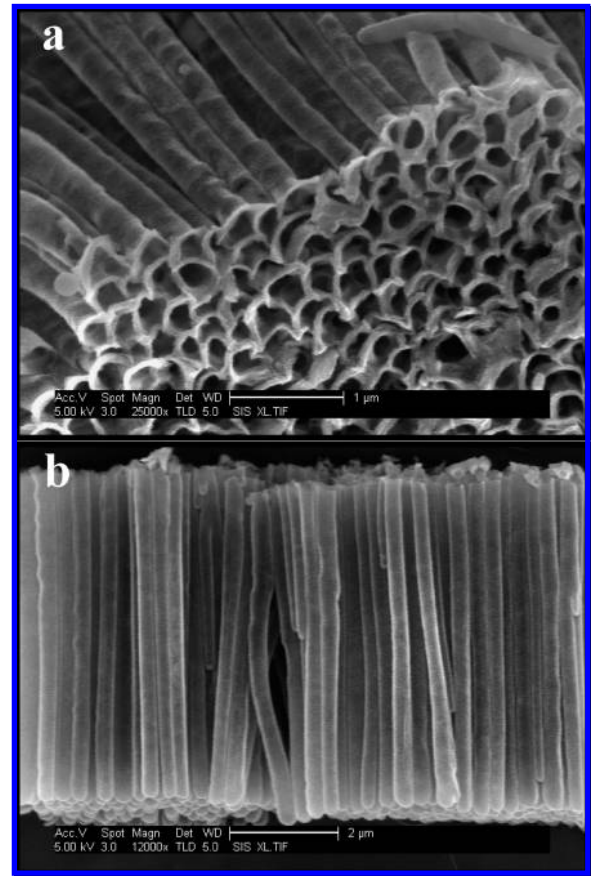

Figure 2. Field emission−SEM images of (a) top-down and (b) side views of TiO_2 nanotube arrays after removal of the anodized alumina template. The average TiO_2 nanotube outer diameter and length are 295 nm and 6.1 μm, respectively.

In order to prepare free-standing TiO_2 nanotubes for eventual device fabrication, the alumina template was removed by selective chemical etching in a solution of 3 M NaOH for 13 min. After complete removal of the alumina template, highly ordered TiO_2 nanotube arrays such as those shown in Figure 2 remain on the aluminum. For this particular example, the average external diameter, tube length, and wall thickness are 295 nm, 6.1 um, and 21 nm, respectively. However these parameters can easily be manipulated by varying the anodization voltage, anodization time, and number of infiltration steps, and studies are currently underway to fully exploit this feature. Additionally, the tube-to-tube spacing is estimated to be approximately 300 nm, which is approximately the same as the external tube diameter due to the fact that they are bundled together and in intimate contact with each other. This should be compared to the pore-to-pore spacing of approximately 430 nm that originally existed in the alumina template. Clearly, upon removal of the template, the tubes do not "fall over"

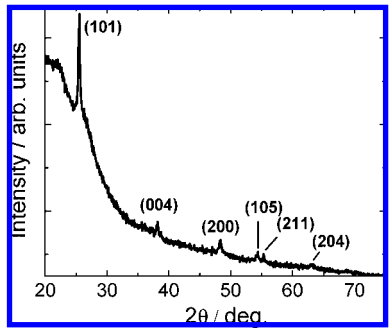

Figure 3. X-Ray diffraction pattern of a TiO_2 nanotube array on an aluminum substrate after removal of the alumina template.

as might be expected. Instead, they bundle tightly together and remain oriented perpendicular to the aluminum substrate in a highly ordered fashion. The aggregation of the tubes on the surface is presumably a result of the attractive van der Waals interactions that exist between tubes and is analogous to the "roping" that is observed in carbon nanotubes. From Figure 2a, it can be seen that the tops of the tubes remain open, while Figure 2b shows that the bottoms are clearly capped due to the conformal coverage of the bottom of the template pores. During the etching procedure, the barrier layer at the bottom of the pores is completely removed resulting in a physical adsorption of the tubes onto the aluminum substrate.

Because the film has been heat-treated at 500 °C for 30 min, the nanotubes have been converted to crystalline titania in the anatase phase. This is demonstrated in Figure 3, which shows the X-ray diffraction pattern of the TiO_2 nanotube arrays standing on the aluminum substrate after removal of the alumina template. The spectrum consists of a variety of peaks that are completely attributable to either anatase TiO_2 or aluminum (the substrate), as indicated. The presence of the peak at 25.45° (anatase) and the absence of one at 27.45° (rutile) indicates that the nanotubes consist entirely of the anatase phase. Note that the broad amorphous background seen in the figure is due to the Kapton tape used during the measurement.

Having preferentially removed the alumina template, the nanotubes can be removed from the aluminum and transferred onto a separate substrate. Adhesive tape is applied to the top surface of the film and when removed, the nanotubes are easily detached from the aluminum substrate. This is demonstrated in Figure 4, which shows three different magnifications of the TiO_2 nanotubes that have been transferred onto an adhesive carbon tape. The "bottom" of the tubes is now presented as the "top" surface and the fact that this end of the tubes is closed is clearly evident. The nanotubes are still highly aligned perpendicular to the substrate indicating that the process of transferring the tubes to another substrate does not disrupt the order to a great extent. Figure 4c also illustrates the fact that over a larger area, the film exhibits a "mud-cracked" surface texture. This is simply caused by the removal of the alumina template. When the template is preferentially etched away, the volume it had occupied becomes void space and the tubes aggregate due to their attractive van der Waals forces. The surface

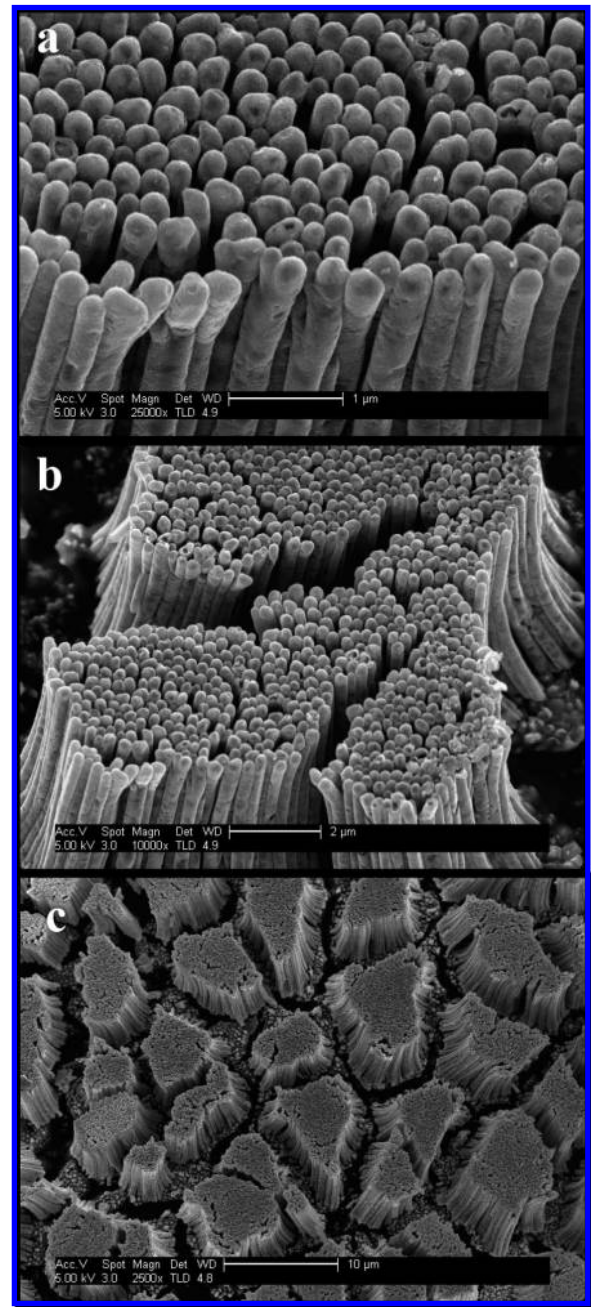

Figure 4. Field emission−SEM images of the TiO_2 nanotubes that have been transferred onto an adhesive carbon tape.

accommodates the void space by creating this mud-cracked surface texture.

The tubes can subsequently be transferred onto a transparent electrode substrate for the fabrication of dye-sensitized solar cells. A schematic representation (not to scale) of the device structure used in these studies is presented in Figure 5. The substrate (fluorine-doped tin oxide (FTO) coated glass) is first prepared by depositing a thin layer of a nanocrystalline (NC) TiO_2 paste onto the FTO in order to promote adhesion of the titania nanotubes to the surface. This coating is similar to the mesoporous titania films used by others in the preparation of standard dye-sensitized cells with the exception that it is much thinner. The procedure used herein is described in the work by Grätzel and co-workers[32] in which

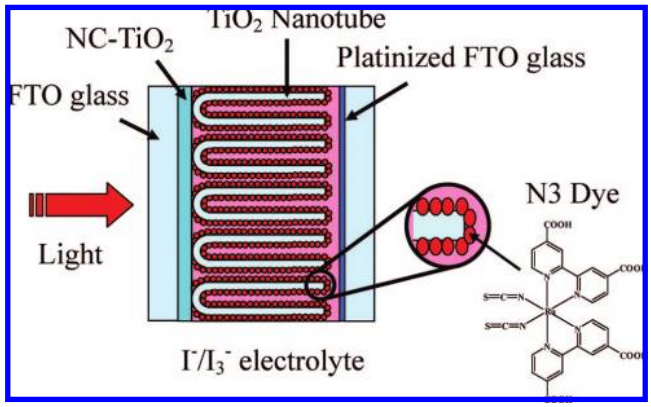

Figure 5. Schematic representation of the architecture used to fabricate devices utilizing the TiO_2 nanotube arrays.

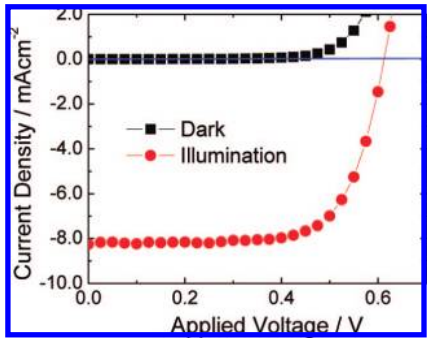

Figure 6. Current−voltage characteristics for a TiO_2 nanotube-based device in the dark (black square) and under illumination (red circle).

they used approximately 10 μm thick films. In this work, films of only 0.2 μm were used solely to act as an interfacial modification layer to promote adhesion. The titania nanotubes are then applied to the substrate such that the closed end is nearest the FTO, as shown in the figure. The adhesive tape that was used to transfer the nanotubes is subsequently "burned off" by heat-treating the film at 500 °C for 30 min in air. The resulting films were then assembled into devices using standard approaches for dye-sensitized solar cells. Namely, the films were sensitized by immersing them for approximately 24 h in a 0.3 mM *t*-butanol/acetonitrile solution (1:1 volume ratio) of the standard ruthenium-based N3 dye, *cis*-bis(isothiocyanato) bis(2,2′-bipyridyl-4,4′-carboxylato)-ruthenium(II). The electrolyte used contained 0.5 M LiI, 0.05 M I_2, and 0.5 M *tert*-butylpyridine in acetonitrile and valeronitrile (1:1 in volume ratio). Finally, platininized FTO-glass was used as the counter electrode and was separated from the substrate by the use of a 100 μm thick Parafilm spacer.

Representative current−voltage ($I-V$) measurements are shown in Figure 6 for a device with an average titania nanotube outer diameter, length, and wall thickness of 295 nm, 15.3 μm, and 42 nm, respectively. The active area of the device was 6.33 mm^2. Upon illumination under AM1.5G conditions (Oriel 300 W solar simulator, 100 mW/cm^2), the device exhibited an open-circuit voltage (V_{oc}) of 0.61 V, a short-circuit current density (J_{sc}) of 8.26 mA/cm^2, and a fill factor (FF) of 0.70, giving an overall power conversion

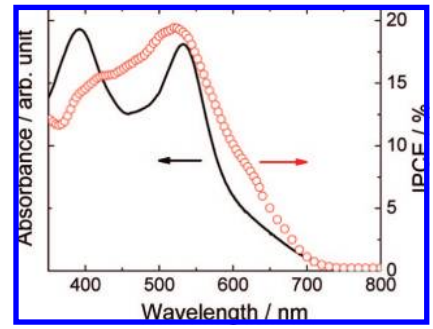

Figure 7. Incident photon-to-current conversion efficiency (IPCE) of a TiO_2 nanotube-based device (open circles) and the solution absorption spectrum of the N3 dye (solid line).

efficiency (η) of 3.5%. The incident photon-to-current conversion efficiency (IPCE) spectrum for the device was measured by scanning monochromatic light chopped at 21 Hz and measuring the induced photocurrent (SRS SR570 current sensitive preamp connected to an EG and G PAR 5210 dual phase lock-in amplifier). As shown in Figure 7, the IPCE exhibits a peak of about 20% at 520 nm as well as small shoulders at 415 and 620 nm. This is in relatively close agreement with the expected maximum based on the accompanying absorption spectrum for the N3 dye, which has local maxima at 392 and 533 nm, both corresponding to a metal-to-ligand charge transfer transition.

These results can be compared to those for standard dye-sensitized solar cells utilizing a mesoporous titania electrode fabricated from commercially available TiO_2 nanoparticles approximately 25 nm in diameter (Degussa AG, P25). For devices made with an 8 μm thick titania film, the fill factor (FF = 0.73) is comparable, while the voltage (V_{oc} = 0.7 V), current density (J_{sc} = 18 mA/cm^2), and power conversion efficiency (η = 10%) are generally higher than those observed here.[33] In addition, the IPCE is close to 90% at 520 nm for a device using a 12 μm thick titania film. The discrepancies between these results can be understood from a consideration of the detailed structure of the titania electrodes. Specifically, the "roughness factor" is a measure of the amount of total internal surface area that is available for dye adsorption relative to its projected surface area. For devices made using the commercially available TiO_2 nanoparticles, this value is typically on the order of 1000.[25] That is to say, the effect of creating the mesoporous titania electrode structure is to increase the total surface area available for dye adsorption by about three orders-of-magnitude. For the nanotube electrodes shown here, the roughness factor can be estimated by calculating the geometrical surface area of the nanotubes and their area density. For nanotubes with an outer diameter of 295 nm, a wall thickness of 42 nm, and a length of 15.3 μm, the total surface area per tube (both internal and external surfaces) is approximately 24 μm^2. Within the template, the tubes are roughly organized in a hexagonal arrangement with a pore-to-pore (or tube-to-tube) spacing of approximately 430 nm, leading to an area density of 6.2 tubes/μm^2 (or 0.16 μm^2 of projected surface area per tube). The ratio of these two numbers (24:0.16) then leads to an estimated roughness factor

of approximately 150. It should be noted that in the films used for device fabrication, the alumina template has been removed and the tubes aggregated, which would result in a local area density of tubes that is higher than the value used here. However, the mud-cracked surface texture shown above accounts for this by having areas with no tubes. Over the relatively large area used for device testing, the average value will be that calculated using the pore-to-pore spacing of the template.

The effect of the significantly lower surface area (roughness factor of 150 versus 1000) that is available for dye adsorption can be seen by considering that the IPCE of the active device can be expressed by the following equation:

$$\mathrm{IPCE}(\lambda) = \mathrm{LHE}(\lambda)\phi_{\mathrm{inj}}\eta_{\mathrm{c}} \quad (1)$$

where LHE = the light harvesting efficiency, φ_{inj} = the quantum yield of charge injection, and η_{c} = the efficiency of collecting the injected charge at the back contact. In dye-sensitized solar cells fabricated using commercially available titania nanoparticles, it has been demonstrated that all three of these values are close to unity in a wavelength region around 520 nm resulting in the high IPCE values that are observed.[25] For the nanotube films shown here, a major effect of the lower roughness factor is a decrease in the LHE of the device, given by

$$\mathrm{LHE}(\lambda) = 1 - 10^{-\Gamma\sigma(\lambda)} \quad (2)$$

where Γ = the number of moles of sensitizer per cm^2 of projected surface area of the film, and σ = the absorption cross section (cm^2/mol), which is obtained from the extinction coefficient (M^{-1} cm^{-1}) of the dye by multiplying by 1000 cm^3/L. Dye-sensitized cells made with commercially available TiO_2 nanoparticles have reported values of Γ and σ of 1.3×10^{-7} mol/cm^2 and 1.42×10^{7} cm^2/mol, respectively, resulting in an LHE of 98%.[25] While the value of σ is a characteristic of the dye and will therefore be the same here, the value of Γ will be significantly reduced as a direct result of the lower surface area. Since the available surface area is reduced to the same extent as the roughness factor (150:1000 = 0.15), the value of Γ is estimated to be 2×10^{-8} mol/cm^2 in these nanotube-based devices, which results in an estimated LHE (and consequently IPCE) of about 47%. The fact that this value is close to twice that observed experimentally suggests that only half of the total nanotube surface area is available for dye adsorption. This is consistent with the nanotubes being aggregated together, thereby prohibiting the dye from accessing the exterior surface. Clearly, a more precise value for Γ would result in a better understanding of device performance. However, this analysis demonstrates that the observed values for the IPCE (20%) and the power conversion efficiency (3.5%) is lower than that for cells made with commercially available TiO_2 nanoparticles largely as a result of a decrease in the amount of available surface area. Improved device performance can therefore be achieved by increasing this value (e.g., reducing nanotube diameter).

In summary, the successful fabrication of TiO_2 nanotubes of variable geometry using an alumina templating method has been demonstrated. By using a mixture of $Ti(OC_3H_7)_4$ and ethanol, extremely uniform infiltration of the pores was achieved resulting in highly aligned TiO_2 nanotubes. TiO_2 nanotubes consisting entirely of the anatase phase were used to fabricate first generation DSSCs. Power conversion efficiencies as high as 3.5% with a maximum IPCE of 20% at 520 nm were achieved. Given the significantly reduced internal surface area compared to traditional nanoparticle-based devices, these results suggest a promising approach to achieve high efficiency devices.

References

(1) Nazeeruddin, M. K.; De Angelis, F.; Fantacci, S.; Selloni, A.; Viscardi, G.; Liska, P.; Ito, S.; Takeru, B.; Grätzel, M. *J. Am. Chem. Soc.* **2005**, *127*, 16835.
(2) Fujishima, A.; Rao, T. N.; Tryk, D. A. *J. Photochem. Photobiol.* **2000**, *C1*, 1.
(3) Grätzel, M. *Nature* **2001**, *414*, 338.
(4) Skryshevsky, V. A.; Vikulov, V. A.; Tretiak, O. V.; Zinchuk, V. M.; Koch, F.; Dittrich, Th. *Phys. Status Solidi A* **2003**, *197*, 534.
(5) Keshmiri, M.; Troczynski, T. *J. Non-Cryst. Solids* **2003**, *324*, 289.
(6) Gong, D. W.; Grimes, C. A.; Varghese, O. K. *J. Mater. Res.* **2001**, *16*, 331.
(7) Chu, S. Z.; Inoue, S.; Wada, K.; Hishita, S.; Kurashima, K. *J. Electrochem. Soc.* **2005**, *152*, B116.
(8) Masuda, H.; Kanezawa, K.; Nakao, M.; Yokoo, A.; Tamamura, T.; Sugiura, T.; Minoura, H.; Nishio, K. *Adv. Mater.* **2003**, *15*, 159.
(9) Wijnhoven, J. E.; Vos, W. *Science* **1998**, *281*, 802.
(10) Wang, W. Z.; Varghese, O. K.; Paulose, M.; Grimes, C. A. *J. Mater. Res.* **2004**, *19*, 417.
(11) Hoyer, P. *Langmuir* **1996**, *12*, 1411.
(12) Chen, Y. S.; Crittenden, J. C.; Hackney, S.; Sutter, L.; Hand, D. W. *Environ. Sci. Technol.* **2005**, *39*, 1201.
(13) Gong, D.; Grimes, C. A.; Varghese, O. K.; Hu, W.; Singh, R. S.; Chen, Z.; Dickey, E. C. *J. Mater. Res.* **2001**, *16*, 3331.
(14) Mor, G. K.; Varghese, O. K.; Paulose, M.; Shankar, K.; Grimes, C. A. *Sol. Energy Mater. Sol. Cells* **2006**, *90*, 2011.
(15) Mor, G. K.; Varghese, O. K.; Paulose, M.; Mukherjee, N.; Grimes, C. A. *J. Mater. Res.* **2003**, *18*, 2588.
(16) Cai, Q.; Paulose, M.; Varghese, O. K.; Grimes, C. A. *J. Mater. Res.* **2005**, *20*, 230.
(17) Mor, G. K.; Shankar, K.; Paulose, M.; Varghese, O. K.; Grimes, C. A. *Nano Lett.* **2005**, *5*, 191.
(18) Paulose, M.; Shankar, K.; Yoriya, S.; Prakasam, H. E.; Varghese, O. K.; Mor, G. K.; Latempa, T. A.; Fitzgerald, A.; Grimes, C. A. *J. Phys. Chem. B* **2006**, *110*, 16179.
(19) Mor, G. K.; Shankar, K.; Paulose, M.; Varghese, O. K.; Grimes, C. A. *Nano Lett.* **2006**, *6*, 215.
(20) Kang, S. H.; Kim, J-. Y.; Kim, Y.; Kim, H. S.; Sung, Y-. E. *J. Phys. Chem. C* **2007**, *111*, 9614.
(21) Zhu, K.; Neale, N. R.; Miedaner, A.; Frank, A. J. *Nano Lett.* **2007**, *7*, 69.
(22) Zhu, K.; Vinzant, T. B.; Neale, N. R.; Frank, A. J. *Nano Lett.* **2007**, *7*, 3739.
(23) Kuang, D.; Brillet, J.; Chen, Peter; Takata, M.; Uchida, S.; Miura, H.; Sumioka, K.; Zakeeruddin, S. M.; Grätzel, M. *ACS Nano* **2008**, *2*, 1113.
(24) Law, M.; Greene, L. E.; Johnson, J. C.; Saykally, R.; Yang, P. *Nat. Mater.* **2005**, *4*, 455.
(25) Feng, X.; Shankar, K.; Varghese, O. K.; Paulose, M.; Latempa, T. J.; Grimes, C. A. *Nano Lett.* **2008**, *8*, 3781.
(26) Limmer, S. J.; Seraji, S.; Wu, Y.; Chou, T. P.; Nguyen, C.; Cao, G. Z. *Adv. Mater.* **2001**, *13*, 1269.
(27) Limmer, S. J.; Chou, T. P.; Cao, G. Z. *J. Mater. Sci.* **2004**, *39*, 895.
(28) Liu, S.; Huang, K. *Sol. Energy Mater. Sol. Cells* **2005**, *85*, 125.
(29) Chu, S.-Z.; Wada, K.; Inoue, S.; Todoroki, S. *Chem. Mater.* **2002**, *14*, 266.
(30) Ohsaki, Y.; Masaki, N.; Kitamura, T.; Wada, Y.; Okamoto, T.; Sekino, T.; Niiharab, K.; Yanagida, S. *Phys. Chem. Chem. Phys.* **2005**, *7*, 4157.
(31) Brinker, C. J.; Scherer, G. W. *Sol-Gel Science*; Academic Press: New York, 1990.
(32) Wang, P.; Zakeeruddin, S. M.; Comte, P.; Charyet, R.; Humphry-Baker, R.; Grätzel, M. *J. Phys. Chem. B* **2003**, *107*, 14336.
(33) Nazeeruddin, M. K.; Kay, A.; Rodicio, L.; Humpbry-Baker, R.; Miiller, E.; Liska, P.; Vlachopoulos, N.; Grätzel, M. *J. Am. Chem. Soc.* **1993**, *115*, 6382.

NL802818D